

A theoretical approach to the propagation of interacting cracks

P. Baud and T. Reuschlé*

EOST, CNRS EP0533, Laboratoire de Physique des Matériaux, 5 rue René Descartes, 67084 Strasbourg Cedex, France.

E-mail: treuschle@eost.u-strasbg.fr

Accepted 1997 April 8. Received 1997 April 8; in original form 1996 June 18

SUMMARY

We propose a scheme to compute interaction effects between two randomly oriented cracks under compressive stresses and we discuss the role crack interactions play in the crack coalescence process. Stress intensity factors are computed by using an iterative technique based on the method of successive approximations. Once crack propagation occurs, curved wing cracks grow from the initial crack tips. The stress intensity factors at the wing crack tips are calculated as the sum of two terms: a component for a single wing crack subjected to both the applied stresses and the interaction effect, and a component due to the sliding of the initial crack. We have applied our procedure to various crack geometries. Our results show that interaction effects act on the crack propagation path. For cracks under tension, our approach correctly predicts the curving, hook-shaped paths of interacting cracks that have been observed in various materials. For *en échelon* compressive cracks, interaction effects depend on the geometry of stepping. For right-stepping cracks, no mode I crack coalescence occurs. A mixed-mode propagation criterion may be introduced to check whether coalescing secondary shear fractures initiate. For left-stepping cracks, depending on whether or not there is overlapping, crack coalescence is achieved by tension wing cracks at the inner crack tips. Without overlapping, the growing wing cracks delimit a region where a tensile secondary fracture may develop and lead to coalescence. These results are consistent with previous work and show that our procedure may be now extended to a population of cracks.

Key words: cracked media, cracks, rock fracture.

1 INTRODUCTION

Several arguments suggest that interactions between macrocracks (faults) or microcracks play a major role in the kinematics of the rupture of geomaterials under a compressive state of stress (Brace & Bombolakis 1963; Hoek & Bieniawski 1965; Bombolakis 1973; Horii & Nemat-Nasser 1985). At the field scale, previous studies (see e.g. Segall & Pollard 1980) have shown that fault traces consist of numerous discrete segments commonly arranged as *en échelon* arrays. The stress-field analysis around *en échelon* cracks carried out by Segall & Pollard (1980) proved that the interaction term has a great influence on the further evolution of structures. Interactions can increase or inhibit the further propagation of faults.

At the laboratory scale, experimental studies (Kranz 1979; Horii & Nemat-Nasser 1985) have strongly suggested that nucleation, growth and interactions of microcracks are the

dominant controlling mechanisms of macroscopic failure. Under a compressive state of stress, a single crack produces two tension wing cracks which grow in a stable manner with increasing axial compression, curving towards the direction of axial compression. This process has been well reproduced by simple analytic simulations (Horii & Nemat-Nasser 1985; Ashby & Hallam 1986; Baud, Reuschlé & Charlez 1996). The solutions for more complex crack geometries involving crack interactions generally require iterative techniques (Horii & Nemat-Nasser 1985; Lockner & Madden 1991; Kachanov 1992). No approach has yet succeeded in decomposing and simulating the mechanisms that lead to crack coalescence and to the localization of rupture in loaded samples.

In this paper, we propose a scheme to compute interaction effects between two cracks oriented randomly. Our approach is an extension of the iterative procedure used by Segall & Pollard (1980). By the use of equivalent cracks, we determine the wing crack paths in order to look at evidence of coalescence. One of the major issues is to investigate whether it is possible to justify the appearance of a shearing band as being a consequence of crack interactions and coalescence. This study

* Corresponding author.

will be carried out with a pair of interacting cracks. The results will provide us with several arguments to discuss further applications of the model to a population of cracks.

2 INTERACTION BETWEEN A PAIR OF STRAIGHT CRACKS

Fig. 1 illustrates the geometry of the problem. We consider a homogeneous, isotropic material subjected to uniform normal stresses σ_1 and σ_2 at infinity. Let α be the angle between σ_1 and the horizontal direction, σ_2 being perpendicular to σ_1 . We introduce two cracks of half-lengths a_1 and a_2 and orientations β_1 and β_2 with respect to the coordinate system (\mathbf{I}, \mathbf{J}) . Because interactions create non-uniform stress distributions on the cracks, we divide each crack into n segments. Each segment is subjected to uniform normal and shear stresses and its length depends on the stress gradients, that is the segment is short where the resolved stress gradients are large and long where the stresses are nearly uniform. Adding the stresses for each segment together, we may approximate any arbitrary stress distribution on the crack.

We first quantify the interaction effect for the pre-existing straight cracks. To solve this problem, we use an iterative technique based on the method of successive approximations (Muskhelishvili 1977). Because stresses everywhere in the material are uniquely defined by the boundary conditions, we just have to guarantee that these conditions are fulfilled on each crack during the iterative process. At each step of the process, we determine the stresses (normal and shear) on both cracks by using complex functions. We then correct the stress field to fulfil the boundary conditions (the detailed procedure is given in Appendix A). The final result are the stress intensity factors K_I and K_{II} at the crack tips of both cracks.

Segall & Pollard (1980) have used the same kind of computing scheme. However, in their study they supposed that the resulting shear stresses on cracks could not be greater than the frictional stresses in a compressive regime. With this statement there is no possibility of further propagation of the cracks since the driving force of the propagating cracks is the difference between shear and frictional stresses. Because we want to look at the propagation of the interacting cracks, we have to work with the effective shear stress on the crack

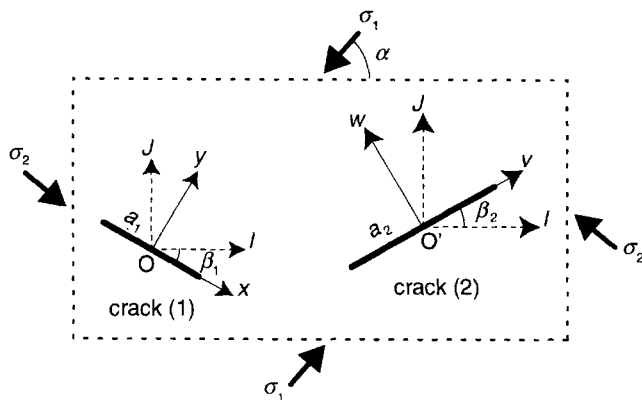


Figure 1. A solid, containing two cracks of half-lengths a_1 and a_2 and orientations β_1 and β_2 , is subjected to stresses σ_1 and σ_2 . Coordinate systems $(O, \mathbf{x}, \mathbf{y})$ and $(O', \mathbf{v}, \mathbf{w})$ are attached to cracks (1) and (2) respectively.

surfaces. At each step, a calculation of the displacements at the crack surfaces allows one to determine the crack aperture, and to make the necessary distinction between closed and open cracks, since the boundary conditions are not the same for both cases. In particular, friction has to be considered for closed cracks. The final scheme works for all configurations and leads to consistent results in the limiting case of pure shear when compared with the results of a previous study by Isida (1973) who used Laurent series.

Fig. 2 gives an example of a left-stepping *en échelon* pair of cracks under biaxial compression. The evolution of the mode II stress intensity factor K_{II} versus the relative horizontal spacing d/a shows that interaction plays an important role when the crack spacing is less than the crack half-length. As expected, K_{II} at the outer crack tip is little affected by d/a . This clearly shows that crack interaction is a short-range process. Before crack tip overlapping, K_{II} is greater than its value K_{II0} for an isolated crack, due to an increase of the shear stress followed by a decrease of the normal compression. When the crack tips overlap, the major effect of interaction is to produce a strong increase of the normal compressive stress, which leads to a lower effective shear stress and a quick decrease of K_{II} . For right-stepping *en échelon* cracks, the effect is reversed because

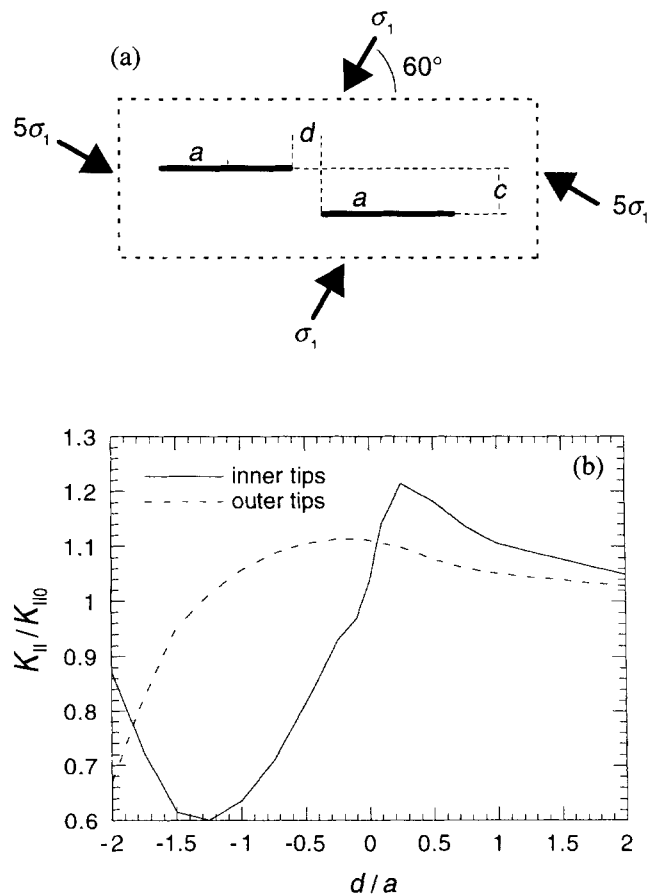


Figure 2. (a) A left-stepping *en échelon* pair of cracks of half-length a is subjected to stresses σ_1 and $5\sigma_1$. The normal distance between cracks is c and the longitudinal distance is d . (b) Normalized mode II stress intensity factor K_{II}/K_{II0} versus relative longitudinal distance d/a for the crack geometry illustrated in (a). K_{II0} is the mode II stress intensity factor for an isolated crack under the same loading conditions.

of the antisymmetry of the normal stress distribution on both cracks.

3 PROPAGATION PATHS OF INTERACTING CRACKS

Once we have calculated the stress intensity factors K_I and K_{II} at each tip of both cracks, we have to look at the propagation condition for both cracks and their further propagation paths. It is well known that when $K_{II} \neq 0$, the relative sliding of the faces of the crack does not result in coplanar crack growth, but rather produces at the tips of the crack curved tension wing cracks which deviate at sharp angles from the sliding plane (Brace & Bombolakis 1963; Hoek & Bieniawski 1965). Thus we have to introduce some modifications in our interaction scheme in order to take into account the possibility of wing crack growth at the tip of the initial straight cracks. Due to interaction effects, the stress intensity factors are not the same at the two tips of an interacting crack (Fig. 2b). It follows that the wing cracks initiated at both tips do not show the same behaviour, which increases the number of parameters because we have to divide the initial crack and both wing cracks into independent sets of segments. In addition, we have to work with small increments of the applied stress to make sure that the associated wing crack growth increment is also small, since interaction can significantly modify the wing crack path. In order to express complex functions for branched cracks, Horii & Nemat-Nasser (1985) introduced distributions of dislocations to work out curved crack extension. However, they only looked at interactions for periodic arrays of cracks. In fact, most of the previous studies (see e.g. Kemeny & Cook 1987) considered periodic arrays of cracks when they dealt with interaction effects on crack propagation. We introduce here an approximate method to determine the propagation paths of two interacting wing cracks.

The starting point of our procedure is the two straight cracks of Fig. 1 in a medium subjected to a horizontal normal stress σ_H and a vertical normal stress σ_V ($\alpha = 90^\circ$). When both stresses are compressive, the cracks are closed and friction has to be introduced. The horizontal stress is held constant and σ_V is increased. We use the previous interaction scheme for straight cracks to determine the stress field on each crack and compute the stress intensity factors at all crack tips. We then use Griffith's criterion (Lawn 1993) for the onset of propagation by introducing the crack extension force G . It is written as $G \geq G_C$, where G_C is the critical crack extension force. G is computed from the stress intensity factors K_I and K_{II} , and is written as $G = (K_I^2 + K_{II}^2)/E$, where E is Young's modulus (Lawn 1993).

At a critical stress level, a wing crack will initiate and grow at one or several tips of the initial straight cracks, depending on where the G value fulfils Griffith's criterion. The direction of propagation is given by the orientation for which G is at a maximum. Because cracks are no longer straight, we have to introduce new expressions for the stress intensity factors. Let us consider the first sliding crack of half-length a being extended by a wing crack at both tips. We replace the curved wing cracks by straight ones (Fig. 3) and let l_r be the length of the right wing crack, and l_l the length of the left one. The orientation relative to the sliding crack is θ_r for the right wing crack and θ_l for the left one (Fig. 4). We now introduce an equivalent straight crack which replaces both sliding and wing

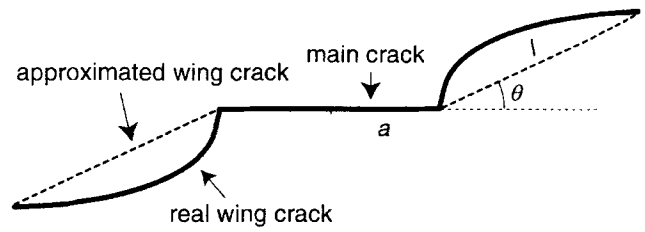


Figure 3. The real wing crack is replaced by a straight one for which the orientation θ depends on its length l .

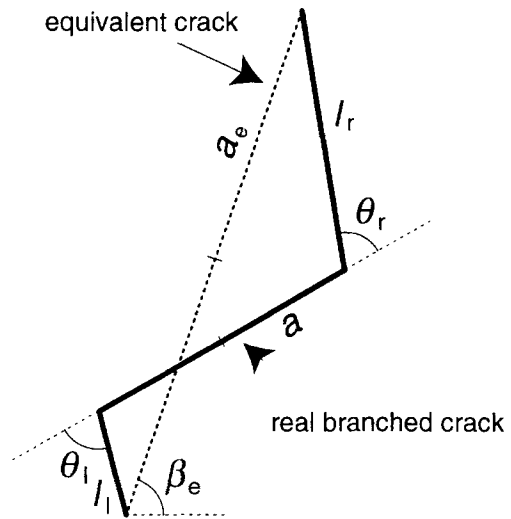


Figure 4. The real crack (sliding crack + wing cracks) is replaced by an equivalent straight crack for which the half-length a_e and the orientation β_e depend on the geometry of the real crack. l_l and l_r (l_l and θ_l) are the length and the relative orientation of the left (right) wing crack.

cracks by joining the tips of the real branched crack (Fig. 4). Its half-length a_e and its orientation β_e depend on the length and orientation of both sliding and wing cracks. By introducing an equivalent crack for the second branched crack too, we are now able to apply the interaction procedure described in Appendix A. As before, we divide each equivalent crack into n segments ($n = 60$) and calculate the normal and tangential stresses applied on each segment of both equivalent cracks.

We then go back to the real branched cracks. We define a new segmentation of these cracks by projecting the segments of the equivalent cracks on the corresponding real cracks (Fig. 5). We assume that the stress components applied on each segment of the real cracks are the same as for the corresponding segment of the equivalent cracks, except that we take into account the orientation difference between both cracks, that is we apply three rotations (one for the sliding crack and two for the wing cracks) to the stress components. As a result we obtain the normal and tangential stresses σ_N and σ_T applied on each segment of the real branched cracks.

We now use a superposition technique to calculate K_I and K_{II} at the tip of a wing crack. We assume that K_I and K_{II} are the sum of two terms: a component $K_I^w(K_{II}^w)$ for a single straight wing crack subjected to both the external stress field and the interaction effect; and a component $K_I^s(K_{II}^s)$ due to the sliding of the initial crack under external and interaction stress fields. This assumption is quite similar to that of Horii &

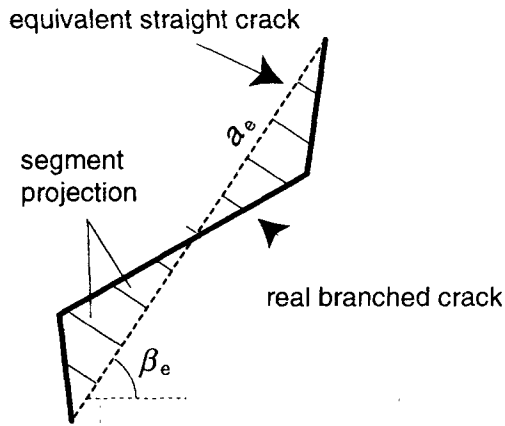


Figure 5. The equivalent crack is divided into segments, which are projected on the real crack to compute the stress components.

Nemat-Nasser (1986), and has been previously developed for a single isolated branched crack (Baud *et al.* 1996).

Let us consider a sliding crack of half-length a and its two associated wing cracks of length l and orientation θ relative to the sliding crack. For determining K_I^w and K_{II}^w we complete each wing crack with a virtual one of the same length, subjected to symmetrical stresses, that is the normal and tangential stresses σ_N and σ_T acting on the virtual wing crack at a distance x to the sliding crack tip are the same as those acting on the real wing crack at the same distance x to the sliding crack tip (Fig. 6). Thus we obtain a crack of length $2l$ whose stress intensity factors K_I^w and K_{II}^w can be written as (Sih & Liebowitz 1968)

$$K_I^w = \frac{1}{\sqrt{\pi l}} \int_{-l}^{+l} \sigma_N(x) \left(\frac{l+x}{l-x} \right)^{1/2} dx, \tag{1}$$

$$K_{II}^w = \frac{1}{\sqrt{\pi l}} \int_{-l}^{+l} \sigma_T(x) \left(\frac{l+x}{l-x} \right)^{1/2} dx.$$

In our case, the integral has to be replaced by a summation over all segments of the wing crack. When the two wing cracks

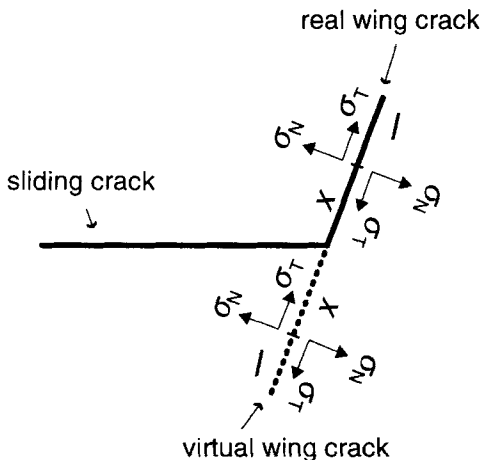


Figure 6. The wing crack is completed with a virtual one of the same length l and subjected to symmetrical stresses, that is the normal and tangential stresses σ_N and σ_T acting on the virtual wing crack at a distance x to the sliding crack tip are the same as those acting on the real wing crack at the same distance x to the sliding crack tip.

do not have the same length, we have to compute K_I^w and K_{II}^w separately for the left and right wing cracks by simply replacing l by the corresponding value in eq. (1): l_l for the left wing crack, l_r for the right one.

The second component $K_I^s(K_{II}^s)$ is calculated by using a procedure very similar to Steif's (1984) approximate solution for a non-infinitesimal branching crack. Steif (1984) proposed replacing the sliding crack and its two wing cracks by a single straight crack of the same orientation as the initial sliding crack and of length $2(a+l)$. This crack is subjected along its entire length to the same normal and tangential stresses N and T as the initial sliding crack. This leads to stress intensity factors K_I and K_{II} of the form $N\sqrt{\pi(a+l)}$ and $T\sqrt{\pi(a+l)}$, respectively. These factors implicitly include the contributions of the wings subjected to the same stresses N and T , which are respectively of the form $N\sqrt{\pi l}$ and $T\sqrt{\pi l}$. These contributions must obviously be subtracted from the previous factors so that the result represents the only influence of the sliding crack. We propose to modify this approximation slightly by considering that in place of loading the whole length of the straight crack and then subtracting the contributions of the wings, the influence of the sliding crack may be modelled by loading only a central part of length $2a$ of the straight crack of length $2(a+l)$. This approximation has already been used in the case of an isolated sliding crack (Baud *et al.* 1996). The normal and tangential stresses applied to the straight crack are those calculated by the interaction procedure described above. The factors K_I^s and K_{II}^s are then given by (Sih & Liebowitz 1968)

$$K_I^s = \frac{f_{\theta\theta}^{II}(\theta)}{\sqrt{\pi(a+l)}} \int_{-a}^{+a} \sigma_{Teff}(x) \sqrt{\frac{a+l+x}{a+l-x}} dx, \tag{2}$$

$$K_{II}^s = \frac{f_{r\theta}^{II}(\theta)}{\sqrt{\pi(a+l)}} \int_{-a}^{+a} \sigma_{Teff}(x) \sqrt{\frac{a+l+x}{a+l-x}} dx,$$

for closed cracks, and

$$K_I^s = \frac{1}{\sqrt{\pi(a+l)}} \left[f_{\theta\theta}^I(\theta) \int_{-a}^{+a} \sigma_N(x) \sqrt{\frac{a+l+x}{a+l-x}} dx \right. \\ \left. + f_{\theta\theta}^{II}(\theta) \int_{-a}^{+a} \sigma_T(x) \sqrt{\frac{a+l+x}{a+l-x}} dx \right], \tag{3}$$

$$K_{II}^s = \frac{1}{\sqrt{\pi(a+l)}} \left[f_{r\theta}^I(\theta) \int_{-a}^{+a} \sigma_N(x) \sqrt{\frac{a+l+x}{a+l-x}} dx \right. \\ \left. + f_{r\theta}^{II}(\theta) \int_{-a}^{+a} \sigma_T(x) \sqrt{\frac{a+l+x}{a+l-x}} dx \right],$$

for open cracks. In the case of closed cracks, the coefficient of friction μ has been introduced to define the effective tangential stress $\sigma_{Teff}(x)$ as $|\sigma_{Teff}(x)| = |\sigma_T(x)| - \mu|\sigma_N(x)|$, where $\sigma_T(x)$ and $\sigma_N(x)$ are, respectively, the tangential and normal stresses applied on the crack. The weighting functions $f_{\theta\theta}^I(\theta)$, $f_{r\theta}^I(\theta)$ and $f_{\theta\theta}^{II}(\theta)$, $f_{r\theta}^{II}(\theta)$ have been introduced to take into account the effect of the orientation of the wing crack on the stress intensity factors. They are determined by considering the infinitesimal wing crack limit and by identifying our solution with the transformed stress intensity factors defined by Lawn

(1993). We obtain

$$\begin{aligned} f_{\theta\theta}^I(\theta) &= \cos^3(\theta/2), \\ f_{\theta\theta}^{II}(\theta) &= -3 \sin(\theta/2) \cos^2(\theta/2), \\ f_{r\theta}^I(\theta) &= \sin(\theta/2) \cos^2(\theta/2), \\ f_{r\theta}^{II}(\theta) &= \cos(\theta/2)[1 - 3 \sin^2(\theta/2)]. \end{aligned} \quad (4)$$

When the two wing cracks do not have the same orientation and length, we have to compute K_I^* and K_{II}^* separately for the left and right wing cracks by simply replacing l and θ by the corresponding values in eqs (2) or (3): l_l and θ_l for the left wing crack, l_r and θ_r for the right one.

We are then able to calculate the crack extension force G for all crack tips. We add a length increment to the growing wing cracks until the corresponding G value is lower than the critical crack extension force G_C . Once all crack tips are stable, we increase the applied vertical stress σ_v and again follow the previous procedure to compute the new crack lengths.

4 RESULTS AND DISCUSSION

The accuracy of the method has been tested in the case of a single crack. Results obtained for the stress intensity factor are very close to accurate analytic solutions (Baud *et al.* 1996). The difference is always less than 5 per cent in the range of parameters we used. This means that the introduction of the equivalent crack does not disturb the expected behaviour of a single crack. Because the analysis in no way depends on the value of a , we have set the length of both initial cracks to unity for all simulations. The incremental wing crack growth length has been set to $a \times 5 \times 10^{-3}$, whilst the incremental vertical stress increase has been set to 0.01. These values ensure a rather continuous propagation process.

The first example of a propagation path is given in Fig. 7. We show the case of two parallel cracks under uniaxial tension. Without any interaction these cracks would propagate in their own planes. Due to interaction effects, the cracks deviate from the horizontal direction and propagate towards each other after a few increments in the opposite direction. However, this interaction effect is only important if the crack tips are very close, that is the distance between the crack tips should not be greater than the half-length of the cracks. The problem of two cracks under tension has been studied by quite a few authors, e.g. Macdonald, Sempere & Fox (1984); Pollard & Aydin (1984). These authors have used this crack geometry to infer some consequences regarding the structure and evolution of oceanic ridge segments. In fact, Pollard & Aydin (1984) based their discussion on the static stress field around crack tips and made some inferences on the propagation paths of interacting cracks without performing any calculations. However, their conclusions are in qualitative agreement with the analysis developed by Macdonald *et al.* (1984) and based on the boundary-element method introduced by Mills (1981). This method uses arrays of dislocations that simulate a crack tip and allows curved crack propagation. Pollard & Aydin's (1984) main result, when applied to oceanic ridge segments, is that two propagating cracks will tend to develop an overlapping spreading-centre geometry unless they are perfectly aligned. This is due to the fact that the predicted crack paths initially curve away from each other. This result is also obtained from our approach, and Fig. 7 clearly shows the

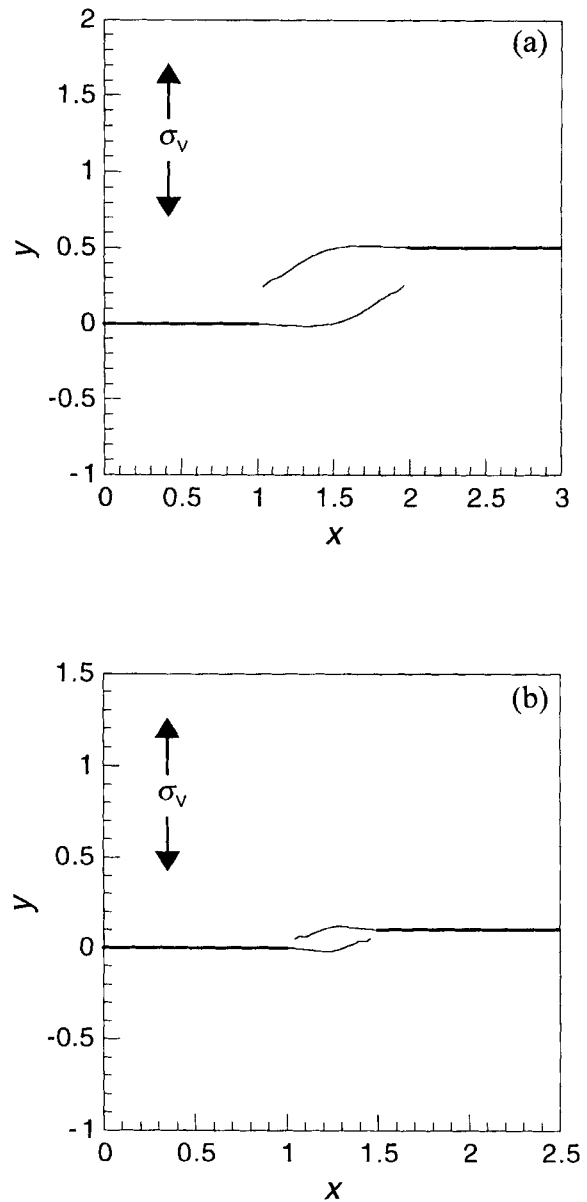


Figure 7. Propagation paths for two parallel cracks of initial half-length $a = 1$ under uniaxial tension. (a) $c = 0.5a$ and $d = a$; (b) $c = 0.1a$ and $d = 0.5a$, where separation d and spacing c are defined in Fig. 2(a).

initial weak divergence of crack paths followed by a strong convergence leading to intersection.

Next we look at *en échelon* cracks by distinguishing left- and right-stepping cracks. This geometry has already been used by several authors to study the brittle fracture process under uniaxial compression. In particular, Bombolakis (1964, 1968) performed compression experiments on photoelastic materials and pointed out that certain *en échelon* arrays of cracks, especially left-stepping arrays, are more favourable for coalescence than others. More recently Spicak & Lokajicek (1986), using perspex plates, and Lin & Logan (1991), using Berea sandstone samples, came to the same conclusion, that left-stepping *en échelon* cracks promote crack coalescence whereas right-stepping cracks hinder this coalescence.

Fig. 8 shows three examples of pairs of left-stepping *en échelon* cracks under uniaxial compression, the parameter

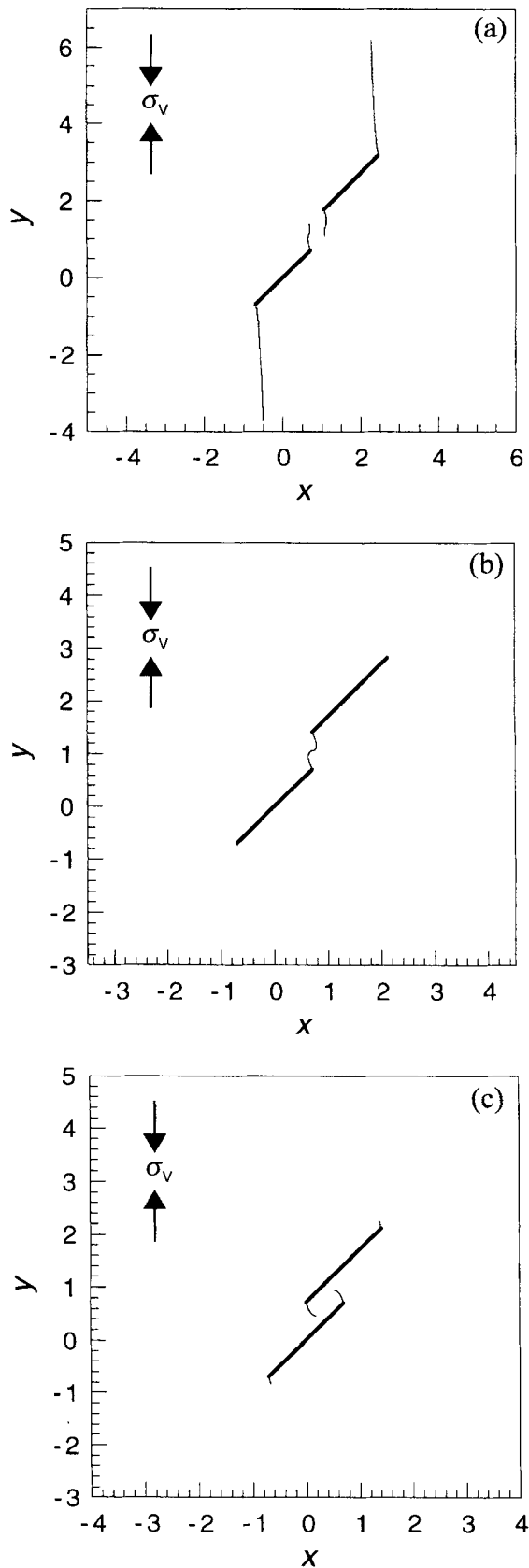


Figure 8. Propagation paths for two left-stepping *en échelon* sliding cracks under uniaxial compression. The initial half-length is $a = 1$ and the orientation is 45° to the horizontal direction. (a) $c = 0.5a$ and $d = a$; (b) $c = 0.5a$ and $d = 0.5a$; (c) $c = 0.5a$ and $d = -0.5a$.

varied being the longitudinal separation between the inner crack tips. We see that the wing crack propagation is disturbed at the inner crack tips, where interaction effects are the strongest. In Fig. 8(a), where the separation is half the length of the cracks, there seems to be no coalescence by the propagation of the inner wing cracks. This result is consistent with a previous calculation by Wei & De Bremaecker (1995b), who used the boundary-element implementation of the repulsion scheme and the maximum strain-energy release-rate criterion (Wei & De Bremaecker 1995a) to compute the growth path of two right-stepping horizontal cracks under right-lateral shearing. Their geometry is comparable with ours since the vertical compression applied on inclined cracks resolves into left-lateral shearing on the crack planes, which makes our geometry of left-stepping cracks under left-lateral shearing the symmetrical geometry of Wei & De Bremaecker's (1995b) one. As they concluded, this geometry may have a geological application since a pull-apart basin may develop in the region confined by the trajectory of the extensions (An & Sammis 1996). At the laboratory scale, Shen *et al.* (1995) observed similar results on a gypsum mixture under uniaxial compression: in a first stage, wing cracks initiate and propagate from the inner crack tips; in a second stage, a secondary fracture originates inside the bridge confined by the wing cracks, propagates towards the pre-existing fracture tips and leads finally to coalescence. This result shows that our model is able to reproduce the first stage of this process, but the second stage cannot be modelled so simply.

In the other two examples, where the longitudinal separation is smaller or negative with overlapping, coalescence occurs directly through the propagation of the wing cracks (Figs 8b and c). When there is no overlapping (Fig. 8b) the wing crack propagation becomes unstable before coalescence takes place, explaining the absence of external wing cracks. This instability is consistent with the experimental results of Horii & Nemat-Nasser (1985) for a suitably oriented row of interacting cracks in Columbia resin. When there is some overlapping (Fig. 8c), an important rotation of the wing cracks takes place and the branching angle becomes greater than 70.5° , the wing crack initiation angle for an isolated sliding crack (Ashby & Hallam 1986). This again is consistent with the experimental results of Spicak & Lokajicek (1986) on perspex plates, especially their group 3 of configuration sets.

Fig. 9 shows two examples of right-stepping *en échelon* cracks with and without overlapping under uniaxial compression. The wing crack path is the same as for an isolated crack, that is interaction does not promote coalescence. This is quite consistent with the results of Spicak & Lokajicek (1986). Indeed, our result agrees well with the morphology of their group 7 of configuration sets. Wei & De Bremaecker (1995b) have applied the boundary-element method to the case of two inclined right-stepping cracks under left-lateral shearing and calculated the initiation angle of the internal wing cracks. Their results are consistent with ours, considering the differences in geometry and stress orientations.

In all cited studies, the crack propagation criterion is based on the maximum strain energy release rate. Another criterion was proposed by Du & Aydin (1993), who decomposed the strain energy into two components: a dilatational strain energy and a distortional strain energy associated respectively with mode I and mode II. They then applied the maximum distortional strain energy criterion for shear fracture propagation

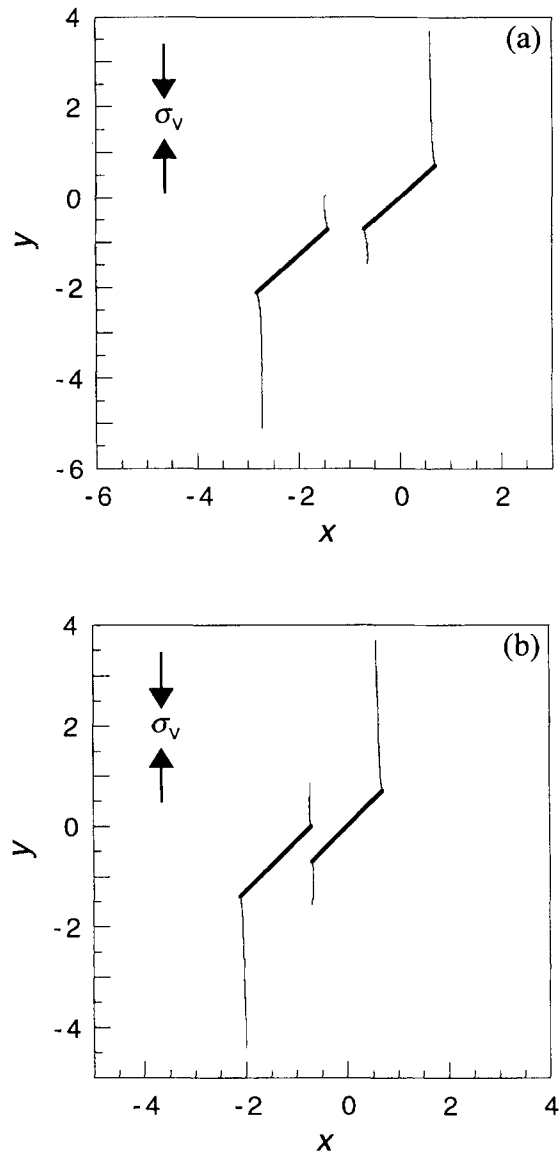


Figure 9. Propagation paths for two right-stepping *en échelon* sliding cracks under uniaxial compression. The initial half-length is $a = 1$ and the orientation is 45° to the horizontal direction. (a) $c = 0.5a$ and $d = 0.5a$; (b) $c = 0.5a$ and $d = -0.5a$.

to the case of left- and right-stepping cracks under biaxial compression. Their conclusion was that two *en échelon* cracks always propagate towards each other, regardless of the sense of shear or crack step direction.

Shen & Stephansson (1993, 1994) proposed another rupture criterion to simulate the mixed-mode fracture propagation. They decomposed the strain energy release rate at a crack tip into the same components as Du & Aydin (1993) but they added a distinction between mode I and mode II fracture toughness for energy (G_{IC} and G_{IIC}). This distinction allowed Shen & Stephansson (1993, 1994) to compute the F -value, which is simply the sum of the normalized values of both strain energy components. For a given material, however, the mode II fracture toughness is much higher than the mode I toughness. For example, in rocks G_{IIC} is found at the laboratory scale to be at least two orders of magnitude higher than G_{IC} (Li 1987). This gap explains the observations by Shen *et al.*

(1995) of coalescence between *en échelon* cracks by secondary shear cracks in addition to the usual mode I wing cracks. In fact, there are two stages in the evolution of the system: in the first stage wing cracks initiate when the dilatational strain energy component G_I reaches the G_{IC} value for a critical stress level; in the second, secondary cracks initiate when the distortional strain energy component G_{II} reaches the G_{IIC} value for a higher critical stress level. The occurrence of secondary shear cracks thus depends on the relative magnitudes of G_{IC} and G_{IIC} .

5 CONCLUSIONS

Our results show that crack interactions play an important role in the crack coalescence process. Nevertheless, interactions only occur over short distances, which means that they need high crack densities in order to become a controlling factor in the fracture process (Horii & Nemat-Nasser 1985). Our results also show that some geometrical requirements have to be fulfilled for the coalescence process to take place. Figs 8 and 9 illustrate the difference between left- and right-stepping *en échelon* cracks. Our result that coalescence is enhanced in the left-stepping geometry is consistent with previous experimental results (Spicak & Lokajicek 1986; Lin & Logan 1991). However, when investigating real rocks, there are some differences between our results and previous experimental observations. In particular, Lin & Logan (1991) used Berea sandstone samples to study the morphology of the interaction zone between two left-stepping *en échelon* cracks. Their experiments revealed the formation of several new sets of fractures within the extensional interaction zone. This complexity cannot be modelled by our approach, nor can it be investigated by photoelastic studies (Bombolakis 1964, 1968), since granular rocks show heterogeneities at the grain scale and inelastic behaviour that cannot be taken into account by these techniques (Bombolakis 1973; Kranz 1979).

Despite these limitations, the theoretical approach we have presented provides a useful tool to simulate the propagation paths of interacting cracks. Although we used an iterative procedure, there is no need for a very powerful computer, and this point makes this approach attractive. The use of equivalent cracks is quite satisfactory since our results are consistent with previous experimental results obtained on homogeneous and elastic materials.

One challenge of our approach was to look at the possibility of the appearance of a shearing macrofracture as a consequence of crack interactions and coalescence. Although this study has been carried out with only a pair of interacting cracks, our results show that under some specific geometries cracks may indeed coalesce and form a longer crack, which in turn may interact with another favourably oriented crack. This is a possible scenario for granular rocks where favourably oriented flawed grain boundaries, or pre-existing well-oriented cleavage cracks are always present. Such a process has been described in detail by Bombolakis (1973) for a pegmatite where fracturing began by the propagation of pre-existing *en échelon* cleavage cracks, and continued by slipping along randomly located but favourably oriented grain boundaries, while the development of partial shear fracture seemed to take place by crack coalescence. A next step in our work will be to look at the coalescence among a population of cracks by separating the

population into pairs of interacting cracks in order to apply our procedure.

ACKNOWLEDGMENTS

We thank Dr De Bremaecker for his helpful comments. This work has been supported by the GDR 914 «Géomécanique des Roches Profondes» of the CNRS.

REFERENCES

- An, L.-J. & Sammis, C.G., 1996. Development of strike-slip faults: shear experiments in granular materials and clay using a new technique, *J. struct. Geol.*, **18**, 1061–1077.
- Ashby, M.F. & Hallam, S.D., 1986. The failure of brittle solids containing small cracks under compressive stress states, *Acta Metal.*, **34**, 497–510.
- Baud, P., Reuschlé, T. & Charlez, P., 1996. An improved wing crack model for the deformation and failure of rock in compression, *Int. J. Rock Mech. Min. Sci. Geomech. Abstr.*, **33**, 539–542.
- Bombolakis, E.G., 1964. Photoelastic investigation of brittle crack growth within a field of uniaxial compression, *Tectonophysics*, **1**, 343–351.
- Bombolakis, E.G., 1968. Photoelastic study of initial stages of brittle fracture in compression, *Tectonophysics*, **6**, 461–473.
- Bombolakis, E.G., 1973. Study of the brittle fracture process under uniaxial compression, *Tectonophysics*, **18**, 231–248.
- Brace, W.F. & Bombolakis, E.G., 1963. A note on brittle crack growth in compression, *J. geophys. Res.*, **68**, 3709–3713.
- Du, Y. & Aydin, A., 1993. The maximum distortional strain energy density criterion for shear fracture propagation with applications to the growth of *en échelon* faults, *Geophys. Res. Lett.*, **20**, 1091–1094.
- Hoek, E. & Bieniawski, Z.T., 1965. Brittle fracture propagation in rock under compression, *Int. J. Fract. Mech.*, **1**, 137–155.
- Horii, H. & Nemat-Nasser, S., 1985. Compression-induced microcrack growth in brittle solids: axial splitting and shear failure, *J. geophys. Res.*, **90**, 3105–3125.
- Horii, H. & Nemat-Nasser, S., 1986. Brittle failure in compression: splitting, faulting and brittle-ductile transition, *Phil. Trans. R. Soc. Lond., A*, **319**, 337–374.
- Isida, M., 1973. Method of Laurent series expansion for internal crack problems, in *Methods of Analysis and Solutions of Crack Problems*, pp. 56–130, ed. Sih, G.C., Noordhoff International Publishing, Leyden.
- Kachanov, M., 1992. Effective elastic properties of cracked solids: critical review of some basic concepts, *Appl. Mech. Rev.*, **45**, 304–335.
- Kemeny, J.M. & Cook, N.G.W., 1987. Crack models for the failure of rocks in compression, in *2nd Int. Conf. Constitutive Laws for Engng. Materials*, pp. 879–887, Tucson.
- Kranz, R.L., 1979. Crack-crack and crack-pore interactions in stressed granite, *Int. J. Rock Mech. Min. Sci. Geomech. Abstr.*, **16**, 37–47.
- Lawn, B., 1993. *Fracture of Brittle Solids*, 2nd edn, Cambridge University Press, Cambridge.
- Li, V.C., 1987. Mechanics of shear rupture applied to earthquake zones, in *Fracture Mechanics of Rocks*, pp. 351–428, ed. Atkinson, B.K., Academic Press, London.
- Lin, P. & Logan, J.M., 1991. The interaction of two closely spaced cracks: a rock model study, *J. geophys. Res.*, **96**, 21 667–21 675.
- Lockner, D.A. & Madden, T.R., 1991. A multiple-crack model of brittle fracture, 1. Non-time-dependent simulations, *J. geophys. Res.*, **96**, 19 623–19 642.
- Macdonald, K., Sempere, J.-C. & Fox, P.J., 1984. East Pacific Rise from Siqueiros to Orozco fracture zones: along-strike continuity of axial neovolcanic zone and structure and evolution of overlapping spreading centers, *J. geophys. Res.*, **89**, 6049–6069.
- Mills, N.J., 1981. Dislocation array elements for the analysis of crack and yielded zone growth, *J. Mat. Sci.*, **16**, 1317–1331.
- Muskhelishvili, N.I., 1977. *Some Basic Problems of the Mathematical Theory of Elasticity*, 2nd edn, Noordhoff International Publishing, Leyden.
- Pollard, D.D. & Aydin, A., 1984. Propagation and linkage of oceanic ridge segments, *J. geophys. Res.*, **89**, 10 017–10 028.
- Pollard, D.D. & Holzhausen, G., 1979. On the mechanical interaction between a fluid-filled fracture and the Earth's surface, *Tectonophysics*, **53**, 27–57.
- Segall, P. & Pollard, D.D., 1980. Mechanics of discontinuous faults, *J. geophys. Res.*, **85**, 4337–4350.
- Shen, B. & Stephansson, O., 1993. Numerical analysis of mixed mode I and mode II fracture propagation, *Int. J. Rock Mech. Min. Sci. Geomech. Abstr.*, **30**, 861–867.
- Shen, B. & Stephansson, O., 1994. Modification of the *G*-criterion for crack propagation subjected to compression, *Eng. Fract. Mech.*, **47**, 177–189.
- Shen, B., Stephansson, O., Einstein, H.H. & Ghahreman, B., 1995. Coalescence of fractures under shear stresses in experiments, *J. geophys. Res.*, **100**, 5975–5990.
- Sih, G.C. & Liebowitz, H., 1968. Mathematical theories of brittle fracture, in *Fracture*, II, pp. 67–190, ed. Liebowitz, H., Academic Press, New York, NY.
- Spicak, A. & Lokajicek, T., 1986. Fault interaction and seismicity: laboratory investigation and its seismotectonic interpretation, *Pure appl. Geophys.*, **124**, 857–874.
- Steif, P.S., 1984. Crack extension under compressive loading, *Eng. Fract. Mech.*, **20**, 463–473.
- Wei, K. & De Bremaecker, J.-C., 1995a. Fracture growth—I. Formulation and implementations, *Geophys. J. Int.*, **122**, 735–745.
- Wei, K. & De Bremaecker, J.-C., 1995b. Fracture growth—II. Case studies, *Geophys. J. Int.*, **122**, 746–754.

APPENDIX A: PROCEDURE FOR INTERACTING STRAIGHT CRACKS

We use the crack geometry illustrated in Fig. 1 and consider two straight cracks indexed (1) and (2). We have first to determine the initial boundary conditions on both cracks, that is we have to define whether cracks are open or closed. Each point of crack (1) is subjected to the normal stress $N^{\infty 1}$ and the shear stress $T^{\infty 1}$ due to the applied external stresses σ_1 and σ_2 . Similarly, crack (2) is subjected to stresses $N^{\infty 2}$ and $T^{\infty 2}$. Crack opening is calculated from the displacements on both cracks. The conformal mapping technique leads to the following expression for the two components u_x and u_y of the displacement vector \mathbf{u} (Muskhelishvili 1977):

$$2M(u_x + iu_y) = \kappa\phi(\zeta) - \frac{\omega(\zeta)}{\omega'(\zeta)}\overline{\phi'(\zeta)} - \overline{\psi(\zeta)}, \quad (\text{A1})$$

where M is the shear modulus, $\kappa = 3 - 4\nu$ (plane strain) or $(3 - \nu)/(1 + \nu)$ (plane stress), where ν is Poisson's ratio. The function $z = \omega(\zeta)$, where $z = x + iy$ and $\zeta = \rho e^{i\theta}$, is introduced to map an ellipse of the real plane ($O, \mathbf{x}, \mathbf{y}$) containing the crack onto a circle of radius ρ in the associated plane (O, ζ_1, ζ_2). In our case the ellipse is a crack of half-length a , and $\omega(\zeta)$ is defined by (Muskhelishvili 1977)

$$\omega(\zeta) = \frac{a}{2} \left(\zeta + \frac{1}{\zeta} \right). \quad (\text{A2})$$

The complex potentials $\phi(\zeta)$ and $\psi(\zeta)$ are obtained as the sum of the contributions of all stressed segments of a crack. Each segment is defined by its extremities $z_1(x_1, y_1)$ and $z_2(x_2, y_2)$, which are associated with τ_1 and τ_2 in the plane (O, ζ_1, ζ_2) respectively. If N and T are the normal and shear

stresses applied to the segment, the elementary potentials for the segment can be written (Pollard & Holzhausen 1979)

$$\begin{aligned} \varphi(\zeta) &= \frac{(N - iT)a}{4i\pi} \left[-\frac{2}{\zeta} \log\left(\frac{\tau_2}{\tau_1}\right) - (\zeta + \zeta^{-1} - \tau_1 - \tau_1^{-1}) \right. \\ &\quad \times \log\left(\frac{\tau_1 - \zeta}{\tau_1^{-1} - \zeta}\right) + (\zeta + \zeta^{-1} - \tau_2 - \tau_2^{-1}) \\ &\quad \left. \times \log\left(\frac{\tau_2 - \zeta}{\tau_2^{-1} - \zeta}\right) \right], \\ \psi(\zeta) &= \frac{Na}{4i\pi} \left[-\frac{4\zeta}{\zeta^2 - 1} \log\left(\frac{\tau_2}{\tau_1}\right) + (\tau_1 + \tau_1^{-1}) \right. \\ &\quad \times \log\left(\frac{\tau_1 - \zeta}{\tau_1^{-1} - \zeta}\right) - (\tau_2 + \tau_2^{-1}) \log\left(\frac{\tau_2 - \zeta}{\tau_2^{-1} - \zeta}\right) \\ &\quad \left. - \frac{(1 + \zeta^2)}{(\zeta^2 - 1)} (\tau_1^{-1} - \tau_1 + \tau_2 - \tau_2^{-1}) \right] \\ &\quad + \frac{Ta}{4\pi} \left\{ \frac{4}{\zeta(\zeta^2 - 1)} \log\left(\frac{\tau_2}{\tau_1}\right) \right. \\ &\quad + \frac{(1 + \zeta^2)}{(\zeta^2 - 1)} (\tau_1^{-1} - \tau_1 + \tau_2 - \tau_2^{-1}) \\ &\quad + [\tau_1 + \tau_1^{-1} - 2(\zeta + \zeta^{-1})] \log\left(\frac{\tau_1 - \zeta}{\tau_1^{-1} - \zeta}\right) \\ &\quad \left. - [\tau_2 + \tau_2^{-1} - 2(\zeta + \zeta^{-1})] \log\left(\frac{\tau_2 - \zeta}{\tau_2^{-1} - \zeta}\right) \right\}. \end{aligned} \quad (\text{A3})$$

We start with crack (2). Its aperture is calculated using eqs (A1) and (A3), where $N = N^{\infty 2}$ and $T = T^{\infty 2}$. If the crack is open, its surface is stress-free, that is the boundary conditions on crack (2) are written

$$\begin{cases} \sigma_{vw}(v) = 0, \\ \sigma_{ww}(v) = 0, \end{cases} \quad \text{for } |v| \leq a_2, w = 0. \quad (\text{A4})$$

In this case, we start the iterative scheme by calculating the stress components induced on crack (1) by the presence of crack (2) loaded by $N^{\infty 2}$ and $T^{\infty 2}$. Otherwise, if crack (2) is closed, friction has to be taken into account by introducing μ , the coefficient of friction. Since crack (2) is closed, the normal stress $N^{\infty 2}$ acting on its surface does not induce any additional stresses on crack (1). It follows that it is only the effective shear stress $|T^{\infty 2}| - \mu|N^{\infty 2}|$ acting on crack (2) that induces stresses on crack (1).

In both cases, the stress components acting on crack (1) are determined using eq. (A3) and the following equations relating stresses to complex potentials:

$$\begin{cases} \sigma_{xx} + \sigma_{yy} = 4 \Re \left[\frac{\varphi'(\zeta)}{\omega'(\zeta)} \right], \\ \sigma_{yy} - \sigma_{xx} + 2i\sigma_{xy} = \frac{2}{\omega'(\zeta)} \Re \left[\bar{\omega} \frac{d}{d\zeta} \left(\frac{\varphi'(\zeta)}{\omega'(\zeta)} \right) + \psi'(\zeta) \right]. \end{cases} \quad (\text{A5})$$

This leads to a normal stress $\sigma_{yy}^{(1)}(x)$ and a shear stress $\sigma_{xy}^{(1)}(x)$ acting on crack (1), which are the first interaction terms. The total stress field acting on crack (1) after the first iteration step is then written as

$$\begin{cases} \sigma_{xy}^T(x) = T^{\infty 1} + \sigma_{xy}^{(1)}(x), \\ \sigma_{yy}^T(x) = N^{\infty 1} + \sigma_{yy}^{(1)}(x). \end{cases} \quad (\text{A6})$$

We determine the aperture of crack (1). This is done using eqs (A1) and (A3), where $N = \sigma_{yy}^T(x)$ and $T = \sigma_{xy}^T(x)$. If crack (1) is open, boundary conditions similar to (A4) have to be fulfilled. It means that we have to counterbalance the excess stresses $\sigma_{yy}^{(1)}(x)$ and $\sigma_{xy}^{(1)}(x)$ by applying stresses of the opposite sign. If crack (1) is closed, we only apply the excess effective shear stress $|\sigma_{xy}^{(1)}(x)| - \mu|\sigma_{yy}^{(1)}(x)|$. As a result we obtain excess stresses $\sigma_{vw}^{(1)}(v)$ and $\sigma_{ww}^{(1)}(v)$ on crack (2) by applying eqs (A3) and (A5). The total stress field acting on crack (2) after the first iteration step is then written as

$$\begin{cases} \sigma_{vw}^T(v) = T^{\infty 2} + \sigma_{vw}^{(1)}(v), \\ \sigma_{ww}^T(v) = N^{\infty 2} + \sigma_{ww}^{(1)}(v). \end{cases} \quad (\text{A7})$$

We now return to crack (2) and apply the same procedure recursively. At each step we calculate the excess stresses applied on both cracks, add them to the total stresses already accumulated on the cracks, and counterbalance them to fulfil the appropriate boundary conditions. We stop the procedure when the excess stresses are less than a given fraction (10^{-5}) of the total stresses. The result of the iterative procedure is the stress field in the solid containing the two interacting cracks. In particular, the stresses acting on the cracks are given by

$$\begin{cases} \sigma_{xy}^T(x) = T^{\infty 1} + \sum_i \sigma_{xy}^{(i)}(x); & \sigma_{yy}^T(x) = N^{\infty 1} + \sum_i \sigma_{yy}^{(i)}(x), \\ \sigma_{vw}^T(v) = T^{\infty 2} + \sum_i \sigma_{vw}^{(i)}(v); & \sigma_{ww}^T(v) = N^{\infty 2} + \sum_i \sigma_{ww}^{(i)}(v). \end{cases} \quad (\text{A8})$$

In order to use this iterative procedure for the computation of the propagation paths of interacting cracks, we have to determine the stress intensity factors K_I and K_{II} for both cracks. They can be written (Sih & Liebowitz 1968)

$$K_I - iK_{II} = 2 \sqrt{\frac{\pi}{a}} \varphi'(\zeta = \pm 1), \quad (\text{A9})$$

where eq. (A3) has been used with $N = \sigma_{yy}^T(x)$ or $\sigma_{ww}^T(v)$, and $T = \sigma_{xy}^T(x)$ or $\sigma_{vw}^T(v)$, depending on the crack we are looking at. The sign $+$ ($-$) holds for the $+$ ($-$) a crack tip.